Materials Chemistry and Physics 240 (2020) 122252

Contents lists available at ScienceDirect

Materials Chemistry and Physics

journal homepage: www.elsevier.com/locate/matchemphys

Graphene oxide modified superconducting and elastic parameters of YBCO superconductor

Bibekananda Sahoo, Anil Kumar Singh, Dhrubananda Behera *

Department of Physics and Astronomy, National Institute of Technology, Rourkela, 769008, India

HIGHLIGHTS

- Addition of GO, leads to increase the grain connectivity and grain growth.
- The superconducting transition temperature increases by increasing wt. % of GO.
- The GO increases the critical current density up to an optimum limit of addition.
- The ultrasonic velocities increase with increasing wt. % of GO.
- The elastic modules also increase with increasing wt. % of GO.

ARTICLE INFO

Keywords:
Critical current density
Pulse-echo technique
Elastic module
Graphene oxide

ABSTRACT

In the present work, (1-x) $YBa_2Cu_3O_{7-\delta}$ + x Graphene Oxide (GO) {x = 0.0, 0.2, 0.4, 0.6 and 0.8 wt %} composite samples were prepared by standard solid state reaction route. The phase purity, structural and morphological analyses of the composite samples were observed through the X-ray powder diffraction and Field emission scanning electron microscopy respectively. The variations of superconducting parameters were observed through the resistivity vs. temperature and electric field vs. current density measurement. The onset of the superconducting transition temperature (T_C^{on}) enhances with increasing wt. % of graphene oxide and the maximum value was found to be 97.02 K for 0.8 wt % graphene oxide added YBCO sample. This may be attributed to the improved inter-linking among the superconducting grains and enhancing the transport of carrier density between the inter-granular sites. As a consequence of the superconducting volume fraction of the composite samples increases, hence critical current density is enhanced with increasing wt. % of graphene oxide. The Ultrasonic measurement has been utilized to observe the elastic parameters of the composite materials.

1. Introduction

Among the various types of high temperature superconductors (HTSc), $YBa_2Cu_3O_{7-\delta}$ (YBCO) is the most attractive superconductor owing to its good physical properties like the higher value of superconducting transition temperature (T_C^{on}), good response towards the higher value of the applied magnetic field and mechanical stability at room temperature [1–4]. But the presence of irregularities, pores, and voids limit the applicability of the parent material towards practical fields like superconducting-magnetic sensors, superconducting wires, tapes etc [5–8]. Hence, several efforts have been made to enhance the superconducting parameters of the bulk sample, which may be accomplished by assimilating the defects acting as artificial pinning centers. The development of artificial pinning centers in HTSc is facilitated by the addition of magnetic impurities, different types of metallic and non-metallic elements, the inclusion of carbon-based compounds, swift heavy ion irradiation and many more [9–13]. As the critical parameters of HTSc are strongly affected by the foreign impurities, hence the nature of the impurities and preparation techniques are the important factors to understand the variation of the critical parameters in HTSc. In order to enhance the critical parameters of the YBCO superconductor, various types of oxide nanoparticles like Al_2O_3, MgO, WO_3, TiO_2, and ZrO_2 etc., have been doped with YBCO [14–16]. Very few reports are available which are based on understanding the role of doping of carbon-based materials on critical parameters of YBCO superconductor [17–19]. Particularly, inclusion of carbon content additives to the YBCO superconductor increases the grain connectivity. Such additives act as good pinning centers since the size of the developed pinning center within the

* Corresponding author.
E-mail address: dbehera@nitrkl.ac.in (D. Behera).

https://doi.org/10.1016/j.matchemphys.2019.122252
Received 7 August 2019; Received in revised form 26 September 2019; Accepted 30 September 2019
Available online 1 October 2019

YBCO matrix is comparable to that of the coherence length of the material. Not only the critical parameters but also the mechanical properties of the HTSc play an important role for suitability of the material in potential applications like superconducting motors, magnetic bearing, and magnetic shields, etc. Hence, it is necessary to understand the variations of elastic parameters like Young's modulus, Bulk modulus, Shear modulus and microhardness, etc of HTSc due to the inclusion of foreign impurities. Few literatures have discussed the variation of elastic moduli due to the addition of oxide and magnetic nanoparticles to HTSc [20–22]. It is already reported that the structural, transport and mechanical strength of the CuTi-1223 superconductor are highly influenced by the inclusion of oxide impurities like SnO_2, In_2O_3, and Fe_2O_3. Similarly, the mechanical strength of the Bi-2212 superconductor is enhanced due to the inclusion of MgO nanoparticles and optimum value is observed for 5.0 wt % MgO doped sample [23]. Better response of elastic module and microhardness of YBCO and Gd-123 superconductors were reported with addition Ag nanoparticles [24]. But the variations of elastic parameters of HTSc YBCO due to the inclusion of carbon-based impurities remain unexplored.

Due to the attractive materialistic properties like good thermal and electrical conductivity, higher values of the elastic moduli and intrinsic mobility, and good barrier potential with impact strength, Graphene oxide (GO) has drawn the attention of the scientific community towards next generation of devices [25,26]. Graphene oxide consists of singular sheets of Graphene enlivened with the functional group of oxygen on the edges and basal plane. The presence of oxygen functional group procreates graphene oxide to be chemically active and mechanically stable. It is also possible that in the sintering process with temperature more than 650 °C, the oxygen in the functional groups of GO is detached and GO reduced into reduced graphene oxide (RGO) [27]. Hence, the removed oxygen enters into the CuO chains of YBCO as a consequence; it leads to the reduction of oxygen vacancies and increases the superconducting parameters.

Here, we report the improved superconducting and elastic parameters of YBCO superconductor due to the addition of graphene oxide. We have also studied the structural, morphological, self-field transport properties, I–V characteristics and ultrasonic measurements of graphene oxide added YBCO sample. The major aspect of this work is to enhance the intergrain boundary connectivity through the weak-link mechanism and improve the superconducting volume fraction by filling the voids and pores.

2. Details of experiment

2.1. Composite sample preparation

The graphene oxide (GO) added $YBa_2Cu_3O_{7-\delta}$ (YBCO) composite samples were prepared by standard solid state reaction technique. The appropriate stoichiometry of Y_2O_3 (Sigma Aldrich 99.9% purity), $BaCO_3$ (Sigma Aldrich 99.9% purity) and CuO (Sigma Aldrich 99.9% purity) were taken and ground for 3 h to achieve the pristine YBCO powder. The above precursor was collected by a crucible and shifted to the programmable furnace for calcination at 850 °C. To achieve the homogeneous YBCO powder, the above procedure was repeated thrice. Ultimately, the YBCO powder was again collected and an appropriate amount of GO (x = 0.2, 0.4, 0.6 and 0.8 wt %) was mixed with YBCO powder through uniform grinding. The graphene oxide is collected in pure phase from sigma Aldrich; hence we have no analysis for characterization of graphene oxide. The composite powder was pressed into a pellet of 13 mm dia. Finally, all pellets were collected in crucibles and transferred to a tubular furnace for the final stage of sintering at 950 °C followed by oxygen annealing for 8 h at 500 °C. Now all the samples were ready for further characterization.

2.2. Characterization technique and measurement

The graphene oxide added YBCO samples were characterized by X-ray diffraction (XRD), Field emission scanning electron microscopy (FESEM), DC transport measurement and ultrasonic measurement. The phase purity and structural analysis of the composite samples were scanned through XRD (Rigaku Ultima-IV X-ray Diffractometer with CuK_α radiation of the wavelength of 1.54 Å) with a step size of 0.02°. The Rietveld refinement analysis gives brief knowledge about the structural parameters and variation in oxygen content of the pure sample due to inclusion of graphene oxide and the refinement data are well analyzed through the Fullprof software. The surface modifications of the specimens are analyzed by FESEM (Model-Nova NanoSEM/FEI with a resolution of 3 nm) analysis. To analyze the size distributions of grains and variation of strain in YBCO matrix under the inclusion of graphene oxide, Williamson-Hall plot (W–H plot) analysis was carried out.

The transport measurement was done with four probe arrangement and liquid helium cryostat. By the help of a temperature controller (LakeShore-332), a constant current source (Keithley 6221) of accuracy $\pm 1.0 \times 10^{-3}$ mA and a nanovoltmeter (Keithley 2182 A) of accuracy $\pm 1.0 \times 10^{-6}$ mV, the resistivity versus temperature measurement was carried out. The two different values of superconducting transition temperature are recorded throughout the measurement. Initially, the onset transition temperature (T_C^{on}) on resistivity vs. temperature plot where the value of resistivity abruptly decreases. Secondly, the offset transition temperature (T_C^{off}) where the resistivity value of the sample almost zero. The electric field versus current density (J_c) measurement was carried out to estimate the variation of critical current density. The value of J_c was measured from the zero voltage value. Before preceding the above measurement, all composite specimens were shaped into the rectangular section of the uniform area of cross-section and silver paste was used for the contact medium.

The ultrasonic pulse-echo technique was utilized to determine the ultrasonic longitudinal wave velocity (V_l) and shear velocity (V_s) at a frequency of 4 MHz under standard atmospheric condition. The bulk density (ρ) of all composite specimens was calculated by the hydrostatic weighing method where toluene acts as a concentration medium. By using the formula $\rho = \left(\frac{M}{V}\right)$, the molar volumes of all specimens were estimated. Here M stands for the molecular weight of the bulk samples in the above relation.

3. Result and discussion

3.1. Structural and microstructural analysis

The powder XRD pattern of graphene oxide (GO) is shown in Fig. 1 (a). The peak indexed at (001) confirms pure phase formation of GO. Similarly, the powder XRD pattern of the pristine YBCO specimen sample is displayed in Fig. 1(b). The peak indexed at (103), (005), (200), (116), and (109) gives satisfactory information about phase purity of the pristine YBCO sample. Few impurity peaks were also observed in pure YBCO sample. A small peak was observed at $2\theta = 30.59°$ corresponds to the secondary phase (impurity phase) Y_2BaCuO_5 [28]. Apart from this, small intense peaks of CuO are marked and labeled with the dollar ($) symbol. The most intense peak of YBCO i.e. (103) shifts towards lower angle, attributes the addition of graphene oxide resulting in the generation of strain inside the YBCO matrix and is depicted in Fig. 1(c). The reflection peaks belong to GO are not illustrious due to the highly dominating phase of YBCO and addition of low wt. % of GO. To analyze the variation of lattice parameters and oxygen contents due to the addition of different wt.% of GO, Rietveld refinement has been carried out through Fullprof software and the pattern is shown in Fig. 1 (d) and (e). All the XRD patterns are fitted well with the theoretical data. The profile residual reliability factor (R_p), Weighted profile residual factor

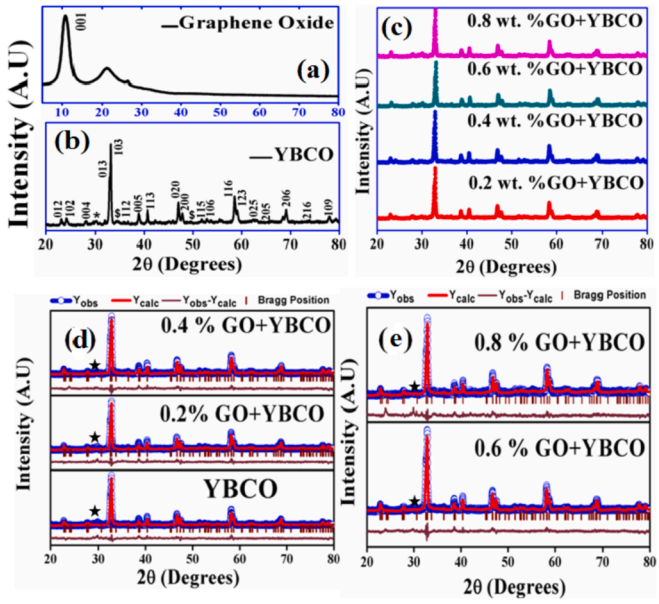

Fig. 1. (a) Displays the XRD pattern of graphene oxide. (b) Shows the XRD pattern of pure YBCO. (c) Shows the XRD pattern of graphene oxide added YBCO samples (x = 0.2, 0.4, 0.6 and 0.8 wt %) added YBCO samples. (d) and (e) Shows Reitveld refinement pattern of graphene oxide (x = 0.0, 0.2, 0.4, 0.6 and 0.8 wt %) added YBCO samples respectively.

(R_{wp}) and goodness of fitting parameters (χ^2) are used as the numerical criterion for fitting. The corresponding values of the lattice parameters, oxygen contents and refinement parameters of the pristine and graphene oxide added sample are tabulated in Table 1. The lattice parameters are slightly varied due to the inclusion of graphene oxide. The considerable reduction of the 'c' lattice parameter is most presumable because of the pressure of apical oxygen bond length by the impact of variation in oxygen contents and the stress developed by GO [29].

The orthorhombic factor was estimated from the formula (b - a)/(b + a). The orthorhombic property of the parent sample increases due to the addition of graphene oxide and clearly, no transformation takes place from orthorhombic to tetragonal phase. The superconducting volume fraction of the sample increases under the addition of GO. As the content of oxygen is a superior parameter which increases the superconducting properties of HTSc, hence the addition of GO to YBCO increases the oxygen content in the parent sample from 6.72 to 6.93.

Fig. 2(a) shows the FESEM micrographs of pure YBCO sample. The pristine YBCO sample shows the well inter-linked rectangular rod-like structure and such rods are uniformly distributed throughout the sample surface. The surface morphology of the graphene oxide is depicted in Fig. 2(b). Fig. 2(c), (d), (e) and (f) and show the FESEM micrographs of 0.2, 0.4, 0.6 and 0.8 wt % GO added YBCO respectively. As observed by addition of graphene oxide, the surface morphology of the composite samples has been changed completely. It is obvious that the inter-linking among the superconducting grains is increased and the degree of porosity is decreased due to the inclusion of GO. But with higher concentration i.e. for 0.8 wt % GO added YBCO sample, the inter-linking among the superconducting grains decreases and the degree of porosity is decreased.

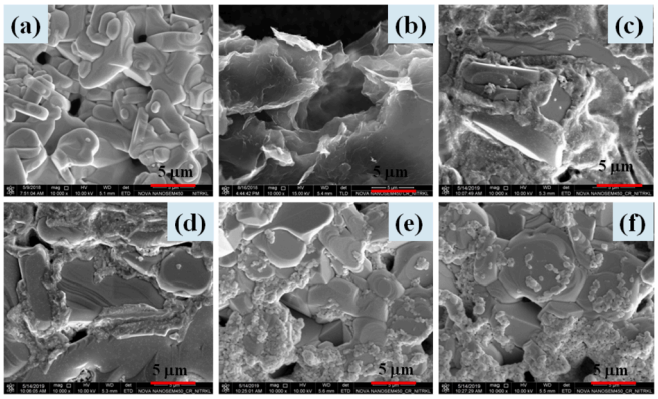

Fig. 2. Displays the FESEM micrographs of all composite samples i.e. (a) pristine YBCO, (b) Graphene oxide (c) 0.2 wt % GO added YBCO (d) 0.4 wt % GO added YBCO, (e) 0.6 wt % GO added YBCO and (f) 0.8 wt % GO added YBCO respectively.

During the synthesis process, when the temperature exceeds a typical value of 600 °C it leads to the removal of oxygen from the functional groups of graphene oxide thereby reduces it to reduced graphene oxide [30]. As an excellent conductive property of RGO encircling YBCO grains improve the connectivity of YBCO grain boundaries that enables easy transport of electrical current [31]. It is inferred from the above concepts that on the reduction of graphene oxide, the eliminated oxygen contributes to the CuO_2 plane as a consequence it leads to enhancement of critical temperature as depicted in Fig. 4 (c) [32].

To investigate the variation of distributions, strain and crystallite size variation within the YBCO superconductor due to the addition of graphene oxide were examined from the Williamson-Hall (W–H) plot [33]. These plots for the composite specimen are shown in Fig. 3. The Williamson-Hall equation is given by

$$\beta_{hkl} = \frac{k\lambda}{D\cos\theta} + 4\varepsilon\tan\theta \quad \text{(A.1)}$$

On further modification, the above equation is represented as

$$\beta_{hkl}\cos\theta = \frac{k\lambda}{D} + 4\varepsilon\sin\theta \quad \text{(A.2)}$$

By plotting a graph between $\beta_{hkl}\cos\theta$ versus $4\sin\theta$, the values of strain component and crystallite size are estimated from the slope (m) and y-intercept (c) respectively. For pristine sample, the crystallite size and strain component are found to be 63 nm and 0.00259 respectively. The component of the strain varies from 0.00245 to 0.00192 due to the addition of GO. It gives clear evidence that the dislocation motion between the superconducting grains is hindered due to increasing wt. % of graphene oxide as inter-granular spacing is filled by the graphene oxide. This emphasizes the presence of graphene oxide improves the grain connectivity which was also evidenced from the surface morphology study. Furthermore, the average crystallite size was found to be increased as 68, 72, 79 and 84 nm for 0.2, 0.4, 0.6 and 0.8 wt % GO added composite samples.

Table 1
The values different parameters obtained from the refinement analysis.

Sample	a (Å)	b(Å)	c(Å)	Vol. (Å)^3	Oxygen content	Ortho. Factor	R_{wp}	R_p	χ^2
YBCO	3.839	3.867	11.689	173.52	6.68	0.0036	7.23	4.18	2.99
0.2 wt % GO + YBCO	3.835	3.870	11.685	173.42	6.77	0.0045	7.84	4.02	3.80
0.4 wt % GO + YBCO	3.837	3.875	11.687	173.76	6.81	0.0049	8.14	4.24	3.81
0.6 wt % GO + YBCO	3.839	3.879	11.674	173.84	6.86	0.0051	7.84	4.02	3.80
0.8 wt % GO + YBCO	3.843	3.881	11.677	174.15	6.94	0.0049	8.12	4.16	3.81

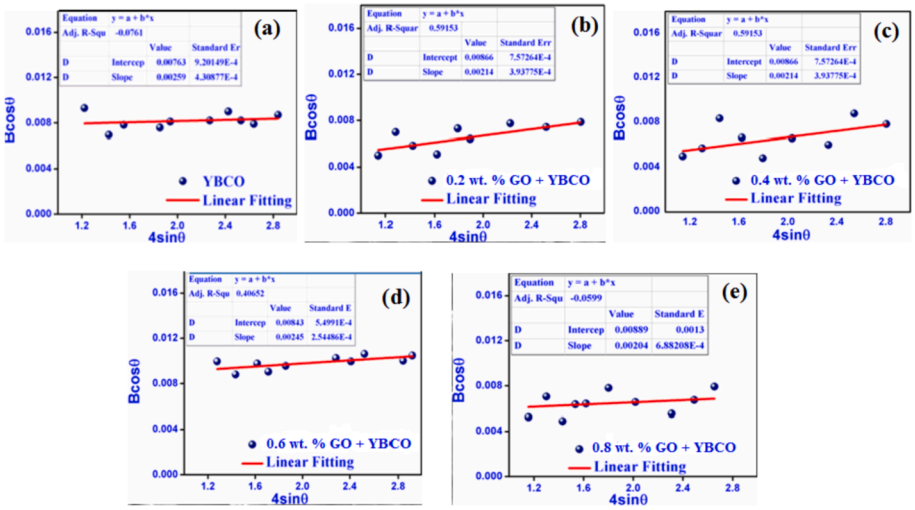

Fig. 3. Display the Williamson-Hall (W–H) plot of the pristine YBCO sample and various wt. % GO added YBCO sample.

3.2. Transport measurement

Fig. 4 (a) displays the variation of resistivity versus temperature plots for graphene oxide (x = 0.0, 0.2, 0.4, 0.6 and 0.8 wt %) added YBCO samples. Before achieving the onset transition temperature (T_C^{on}), all composite samples were showing metallic character. When the temperature falls below T_C^{on}, the resistivity of the samples start decreasing and at temperature T_C^{off}, the resistivity of the samples completely vanished and global superconductivity is established. Fig. 4 (b) shows the temperature dependent derivative versus temperature plot of the composite samples. The value of T_C^{on} is estimated from the uppermost point of the sharp peak of the temperature dependence resistivity versus temperature plot.

The onset critical temperature (T_C^{on}) is enhanced with increasing wt. % of graphene oxide. The variations of the onset transition temperature (T_C^{on}) and the off-set transition temperature (T_C^{off}) are shown in Fig. 4 (c). This may be attributed to the improvement in weak-links between the superconducting grains as graphene oxide nanoparticles occupy the space among the superconducting grains. For pristine sample, T_C^{on} is observed to be 92.18 K. The optimum value of T_C^{on} is found for 0.8 wt % GO added YBCO sample and the value is nearly about 101.02 K. Furthermore, during the sintering process of the sample preparation, the oxygen that attached to the functional group of graphene oxide is removed out and introduced into the CuO chain and is responsible for the enhancement of T_C^{on} [34]. The offset transition temperature (T_C^{off}) of cuprates superconductors depend on the restricted concentration of charge carrier in CuO_2 planes. On the other hand, the charge reservoir layer that provides the charge carriers to the CuO_2 planes also determined from the availability of oxygen contents in this layer. As the addition of graphene oxide increases the oxygen contents of the sample, hence more numbers of charge carriers are available in the CuO_2 plane and hence T_C^{off} increase with increasing wt. % of graphene oxide [35].

The superconducting volume fraction of graphene oxide added sample is increased, as the oxygen content is increased due to the higher

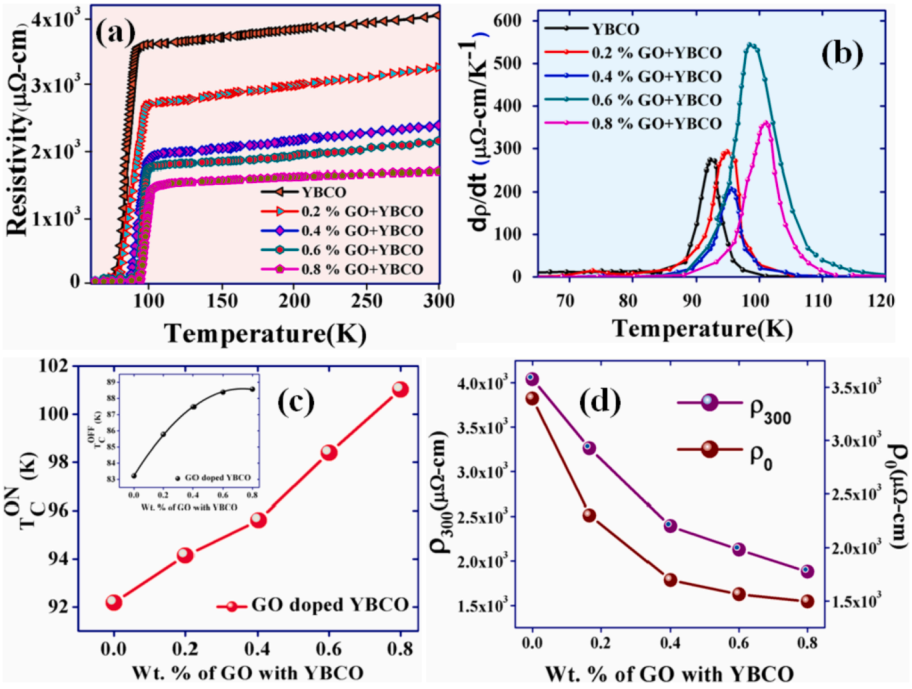

Fig. 4. (a) Displays the resistivity versus temperature plot of graphene oxide (x = 0.0, 0.2, 0.4, 0.6 and 0.8 wt %) added YBCO samples. (b) Displays the variation of temperature derivative of resistivity versus temperature plot to determine the superconducting transition temperature from the sharp peak. (c) Displays the variation of onset critical temperature (T_C^{on}) with the variation of GO added with the YBCO sample and inset shows the variation of offset transition temperature (T_C^{off}) with varying concentration of GO in YBCO sample. (d) Shows the variation of room temperature resistivity and residual resistivity with different concentration of GO with the YBCO sample.

percentage of addition. Hence, the increase of T_C^{off} may be ascribed to the increase in superconducting volume fraction and enhancement of weak-links between the superconducting grains due to the addition of graphene oxide [36]. The normal state resistivity (ρ_{300K}) of pristine YBCO sample is found to be 4.041 mΩ-cm and the value of ρ_{300K} decreases with increasing wt. % of graphene oxide and the same is depicted in Fig. 4 (d). This may be ascribed to the reduction of the scattering cross-section of the charge carriers, as GO resides near the grain boundary. Similarly, the residual resistivity (ρ_0) also decreases with increasing wt. % of graphene oxide.

The value of residual resistivity is obtained from the equation *i.e.* $\rho_n(T) = \rho_0 + \alpha T$. The straight-line fitting of the resistivity versus temperature in between the temperature range 100–300 K, the y-intercept gives the value of ρ_0 and the values are tabulated in Table 2. The value of the residual resistivity mainly depends upon the sample homogeneity and extent of defect created by the foreign impurities [37,38]. But the addition of graphene oxide to the YBCO matrix decreases the above parameters as GO nanoparticles occupy the grain boundary region. Hence, the grain boundary resistance is reduced and the supercurrent flows easily through the materials [39]. Furthermore, the slope of the straight line gives the value of the temperature coefficient of resistivity (α), which mainly depends on the intrinsic interaction between the superconducting grains. The value α is also increased with increasing wt. % of graphene oxide. The value of ΔT is obtained from the difference between the onset and off-set transition temperature. It is found to be 2.97 K for the pristine sample indicating good quality of the pristine sample.

3.3. Current vs. voltage measurement

The electric field versus current density curves for the pristine and graphene oxide added sample is depicted in Fig. 5 (a). The critical current density is estimated from the plot using the principle of 1 μV/cm [40]. The quantity of current density required producing an electric field of unity magnitude and in the units of μV/cm is termed as critical current density. Fig. 5 (b) shows the plot between current density variations with different wt. % of graphene oxide. For the pristine YBCO sample, the measured value is found to be 21.90 A/cm^2. The critical current density is increased with increasing wt. % of graphene oxide up to 0.6 wt % and then it leads to a decrease of J_C as the addition of GO reaches a typical value of 0.8 wt %. The initial increase in critical current density may be ascribed to the increase in superconducting volume fraction and reduction of pores, voids.

As a result of which GO increases better weak-linking among the superconducting grains, leading to enhancement of J_C. But for 0.8 wt % of graphene oxide added YBCO sample, there is an abrupt rise in the porosity of the sample as depicted in Fig. 6 (b) and the content of porosity is mentioned in Table 3. The porosity of the samples is

Table 2
Shows the values of different critical coefficient as obtained from the transport analysis of different concentration of GO to YBCO sample.

Sample	T_C^{on} (K)	T_C^{off} (K)	ρ_0 (μΩ-cm)	ρ_{300} (μΩ-cm)	α (μΩ-cm K^{-1})	ΔT (K)
YBCO	92.18	89.21	3392.48	4040.53	2.36	2.97
0.2 wt % GO + YBCO	94.89	91.78	2446.37	3260.42	2.77	3.11
0.4 wt % GO + YBCO	95.60	92.48	1697.84	2393.11	2.78	3.12
0.6 wt % GO + YBCO	96.30	93.19	1564.28	2129.25	2.79	3.11
0.8 wt % GO + YBCO	97.02	93.89	1409.47	1680.57	2.84	3.13

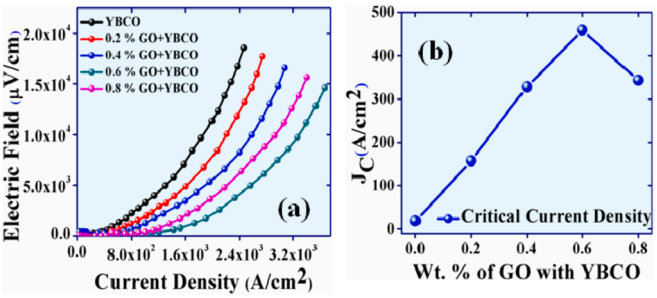

Fig. 5. (a) Displays the electric field versus current density plot for graphene oxide (x = 0.0, 0.2, 0.4, 0.6 and 0.8 wt %) added YBCO samples. (b) Displays the critical current density variation with different concentration of graphene oxide (x = 0.0, 0.2, 0.4, 0.6 and 0.8 wt %).

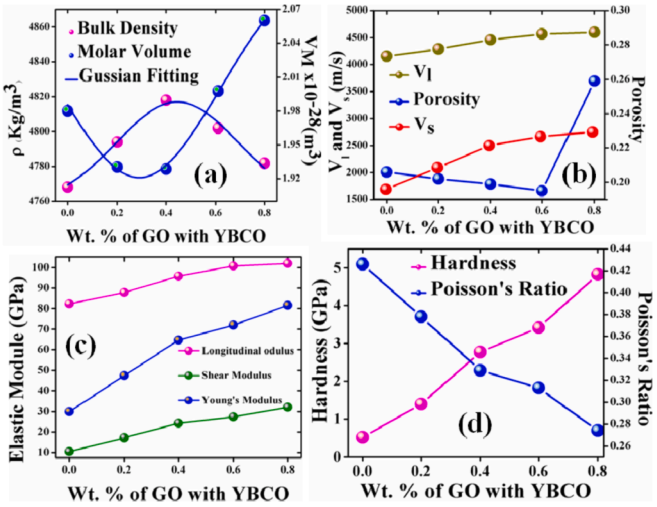

Fig. 6. (a) Displays variation of bulk density and molar volume of graphene oxide (x = 0.0, 0.2, 0.4, 0.6 and 0.8 wt %) added YBCO samples. (b) Shows variation of Porosity (P), longitudinal velocity (V_l), Shear velocity (V_s) of the composite samples. (c) Displays variation of elastic modulus of the composite samples. (d) Displays the variation in hardness and Poisson's ratio of the composite samples.

Table 3
Shows the values of X-ray density (ρ_x), Bulk density (ρ), Porosity (P), Longitudinal velocity (V_l), Shear velocity (V_s), Mean ultrasonic velocity (V_m) and Molar volume (V_M) of graphene oxide (x = 0.0, 0.2, 0.4, 0.6 and 0.8 wt %) added YBCO samples.

Sample	ρ_x (kg/m^3)	ρ (kg/m^3)	P	V_l (m/s)	V_s (m/s)	V_m (m/s)	$V_M \times 10^{-28}$ (m^3)
YBCO	6012	4768	0.206	4154	1484	1686	1.98
0.2 wt % GO + YBCO	6015	4794	0.202	4286	1898	2142	1.94
0.4 wt % GO + YBCO	6019	4818	0.199	4459	2248	2520	1.92
0.6 wt % GO + YBCO	6025	4801	0.195	4568	2383	2666	2.02
0.8 wt % GO + YBCO	6029	4788	0.259	4584	2572	2862	2.06

calculated using the following relation, and hence the supercurrent doesn't found a percolative path to flow throughout the sample.

$$porosity(p) = [1 - Bulk\ density(\rho) / X - Ray\ density(\rho_x)] \quad (B.1)$$

The bulk density is defined as the mass of the many particles of the materials divided by total volume occupied. Here the bulk density of all composite samples has been calculated by the hydrostatic method. The X-ray density can be calculated by using the following relation. i.e. $\rho_x = n.\ M_w/(N_A.V)$. Where n is the number of atoms per unit cell, M_w is the molecular weight, V is the volume of the unit cell and N_A is Avogadro's number.

3.4. Ultrasonic measurement

The variation of molar volume (V_M) and bulk density (ρ) of graphene oxide added YBCO samples are displayed in Fig. 6 (a) and the corresponding values are tabulated in Table 3. The observed value is increased with increasing wt. % of graphene oxide up to 0.6 wt % and then decreases. It may be due to the variation of atomic mass, atomic volume and molecular weight of the different ingredient particles [41]. The variation of longitudinal velocity (V_l) and shear velocity (V_s) with different wt. % of graphene oxide are depicted in Fig. 6 (b). The corresponding values of velocities are increased with increasing wt. % of graphene oxide. Usually, the ultrasonic velocities rely upon the separation between particles or atoms [42,43]. Hence, the rise in longitudinal velocity (V_l) and shear velocity (V_s) with increasing wt. % of graphene oxide results in the decrease in separation between the grains. Furthermore, the enhancement of ultrasonic velocity may be ascribed to the greater connectivity between the superconducting YBCO grains with graphene oxide nanoparticles throughout the samples [44].

On carefully examining Fig. 6 (b), it is obvious that the variation of V_s is much more sensitive than V_l. For lower wt. % graphene oxide added YBCO samples, V_s increases more rapidly than that of the higher doped sample. Since, the addition of GO decreases the porosity of the sample, thereby increasing the connectivity among the superconducting grains and hence these are the most important factors responsible for such type of variation of ultrasonic velocities.

By considering the porosity (P) of the sample, Ultrasonic velocity measurement in HTSc YBCO provides reliable outcomes for both single crystals and doped polycrystalline ceramics [45]. The variation of porosity is observed from the higher density sample to lower dense sample and varies from 0.3% to 0.4%, as reported in the literature. Hence, porosity alone is adequate to clarify the important component in the variation of velocity in ultrasonic measurement [46]. The content of porosity variation with the composite samples is presented in Fig. 6 (b) and respective values are tabulated in Table 3. It is noted that the porosity of the composite sample decreases up to 0.6 wt % of graphene oxide addition and then a remarkable increase in porosity is noticed for 0.8 wt % composite sample. This may be a result of the generation of irregularities, voids in the grain boundaries of YBCO with the further addition of graphene oxide. Such irregularities, voids progressively decrease the superconducting parameters, particularly in HTSc.

To understand the mechanical behavior of the composite samples towards practical application, it is necessary to study the variations of different elastic parameters such as Longitudinal Modulus (L), Modulus of Rigidity (G), Poisson's ratio (σ), Young's Modulus (Y), Hardness (H). By knowing the values of longitudinal velocity (V_l) and shear velocity (V_s), the values of the elastic parameters are calculated by using the following formulas.

$$\text{Modulus of Rigidity}(\mathrm{G}) = \rho V_s^2 \quad (C.1)$$

$$\text{Longitudinal Modulus}(\mathrm{L}) = \rho V_l^2 \quad (C.2)$$

$$\text{Poisson's ratio}\left(\sigma\right) = \frac{L - 2G}{2(L - G)} \quad (C.3)$$

$$\text{Young's Modulus } (Y) = (1 + \sigma)\ 2G \quad (C.4)$$

$$\text{Hardness}\left(\mathrm{H}\right) = \frac{(1 - 2\sigma)Y}{(1 + \sigma)} \quad (C.5)$$

By utilizing the above formula, the elastic moduli of the composite samples are calculated and are mentioned in Table 4. It is noted that the values of elastic moduli gradually increase with increasing wt. % graphene oxide. Such results attributed to the reduction of the voids and irregularities as graphene oxide is diffused near the grain boundaries and pore surfaces. As a result of which the dislocation motion between the superconducting grains are completely hindered and hence, strain factor inside the superconducting matrix is reduced [47].

The microhardness (H) is defined as the amount of stress needed to eliminate the free volume of the solid materials. The microhardness (H) variation with different wt. % of graphene oxide is depicted in Fig. 6 (d). The value of microhardness increases with increasing wt. % graphene oxide. This type of enhancement mainly attributed to the improvement of grain connectivity, reduction of voids and porosity of the superconducting samples and opposes to the formation of cracks on the grain boundary region due to the addition of GO. A comparable pattern of microhardness (H) and Elastic moduli were already reported in several literatures [48,49].

Particularly, to determine the stress and elastic properties of the solid materials towards engineering applications, Poisson's ratio of the specimen sample is a significant requirement. The variation of Poisson's ratio (σ) with different wt. % of graphene oxide is shown in Fig. 6 (d). The behavior of the 'σ' is completely opposite that of the elastic moduli and microhardness i.e. decreases with increasing wt. % of graphene oxide. Such behavior of 'σ' might be due to the variation in connectivity between the superconducting grains due to the addition of graphene oxide [41].

Particularly, in HTSc Debye Temperature (θ_D) provides sufficient information about the major role of phonons in the superconducting matrix. The void-free value of Debye Temperature (θ_D) for cuprate superconductors lies in between 250 K and 500 K [50]. The value of θ_D is calculated by using the following formula [51].

$$(\theta_D) = \frac{h}{k}\left(\frac{3N}{4\pi}\right)^{1/3} Vm \quad (C.6)$$

Here 'h' stands for Plank's constant, 'k' stands for Boltzmann's constant, 'N' stands for the vibrational density of atoms and V_m represents the mean ultrasonic velocity respectively. The variation of Debye Temperature (θ_D) with different wt. % of graphene oxide added sample is depicted in Fig. 7 (a). It is obvious the θ_D increases with increasing wt. % of graphene oxide. The variation of θ_D mainly depends upon the mean ultrasonic velocity and vibrational density of the atoms. As the mean ultrasonic velocity increases with GO concentration (tabulated in Table 3), hence θ_D also increases. The enhancement in value of θ_D confirms that the lattice vibrations are constrained by the inclusion of graphene oxide and completely suppressed for higher wt. %.

Table 4
Display the values of Longitudinal Modulus (L), Modulus of Rigidity (G), Poisson's ratio (σ), Young's Modulus (Y), Hardness (H) and Debye Temperature (θ_D) of graphene oxide (x = 0.0, 0.2, 0.4, 0.6 and 0.8 wt%) added YBCO samples.

Sample	L (GPa)	G (GPa)	σ	Y (GPa)	H (GPa)	θ_D (K)
YBCO	82.27	10.50	0.426	29.94	0.518	267.7
0.2 wt% GO + YBCO	87.80	17.21	0.378	47.43	1.399	284.3
0.4 wt% GO + YBCO	95.79	24.34	0.329	64.69	2.775	299.8
0.6 wt% GO + YBCO	100.82	27.43	0.313	72.03	3.419	311.5
0.8 wt% GO + YBCO	101.99	32.11	0.427	81.56	4.923	326.3

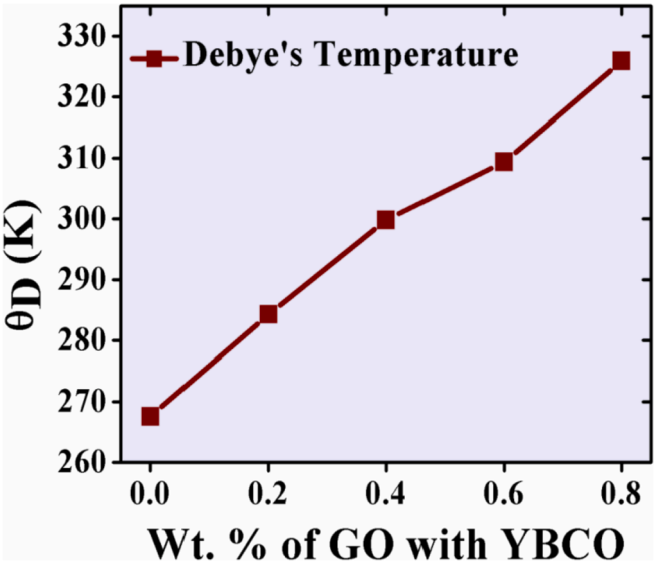

Fig. 7. (a) Shows the variation of Debye Temperature (θ_D) with different wt. % of graphene oxide added YBCO sample.

4. Conclusions

The various wt. % of graphene oxide (x = 0.0, 0.2,0.4,0.6 and 0.8 wt %) added YBCO samples were prepared successfully by standard solid state reaction technique. The orthorhombic structure of the YBCO matrix remains unchanged which gives clear evidence of the presence of graphene oxide near the grain boundary region. The FESEM micrographs display the granular structure with the enhancement of particle size after the addition of graphene oxide. Though the superconducting parameters are increased due to the addition of the graphene oxide, still a restriction in the distribution of graphene oxide is an uncertain aspect. The orderly reduction of room temperature resistivity, residual resistivity and systematic enhancement of onset critical temperature with increasing wt. % of graphene oxide is due to the uniform distribution of graphene oxide near the grain boundary region of YBCO. Particularly, this improvement may be attributed to good interlinked between the superconducting grains, as the irregularities and voids are filled by the graphene oxide. But the superconducting volume fraction begins to decrease after the optimum level of addition of graphene oxide which is responsible for further degradation in critical current density value. The variations of elastic parameters of the composite samples were characterized by Ultrasonic measurement techniques. The Longitudinal Modulus (*L*), Modulus of Rigidity (*G*), and Young's Modulus (*Y*) are increased with increasing wt. % of graphene oxide. It may be attributed to the hindrance of dislocation motion between the superconducting grains as graphene oxide resides near the grain boundary.

Acknowledgment

The authors thank Dr. Anil K. Singh, Department of Physics and Astronomy, National Institute of Technology, Rourkela for providing the oxygen annealing facility for the preparation of the sample. I would like to thanks S.S Nayak, for her support and fruitful discussion during the work. The author (B. Sahoo) is thankful to DST INSPIRE for providing the financial support to carry out this performance under the INSPIRE scheme with sanction number DST/INSPIRE/03/2014/004355 during my research work.

References

[1] R.A. Hawsey, D.K. Christen, Progress in research, development, and pre-commercial deployment of second generation HTS wires in the USA, Phys. C: Supercond. Appl. 445 (2006) 488–495.
[2] S. Dadras, Y. Liu, Y.S. Chai, V. Daadmehr, K.H. Kim, Increase of critical current density with doping carbon nano-tubes in $YBa_2Cu_3O_{7-\delta}$, Phys. C Supercond. 469 (1) (2009) 55–59.
[3] D.M. Gokhfel'd, D.A. Balaev, S.V. Semenov, M.I. Petrov, Magneto resistance anisotropy and scaling in textured high-temperature superconductor $Bi_{1.8}Pb_{0.3}Sr_{1.9}Ca_2Cu_3O_x$. Phys. Solid State 57 (11) (2015) 2145–2150.
[4] A. Öztürk, İ. Düzgün, S. Çelebi, The effect of partial Lu doping on magnetic behavior of YBCO (123) superconductors, J. Alloy. Comp. 495 (1) (2010) 104–107.
[5] W.K. Kwok, U. Welp, A. Glatz, A.E. Koshelev, K.J. Kihlstrom, G.W. Crabtree, Vortices in high-performance high-temperature superconductors, Rep. Prog. Phys. 79 (11) (2016) 116501.
[6] K. De Keukeleere, P. Cayado, A. Meledin, F. Vallès, J. De Roo, H. Rijckaert, , et al. S. Ricart, Superconducting $YBa_2Cu_3O_{7-\delta}$ nanocomposites using preformed ZrO_2 nanocrystals: growth mechanisms and vortex pinning properties, Adv. Electr. Mater. 2 (10) (2016) 1600161.
[7] P.P. Rejith, S. Vidya, S. Solomon, J.K. Thomas, Flux-pinning properties of nanocrystalline HfO_2 added $YBa_2Cu_3O_{7-\delta}$ superconductor, Phys. Status Solidi 251 (4) (2014) 809–814.
[8] D. Dimos, P. Chaudhari, J. Mannhart, Superconducting transport properties of grain boundaries in $YBa_2Cu_3O_7$ bicrystals, Phys. Rev. B 41 (7) (1990) 4038.
[9] T.G. Holesinger, L. Civale, B. Maiorov, D.M. Feldmann, J.Y. Coulter, D.J. Miller, , et al.X. Li, Progress in nanoengineered microstructures for tunable high-current, high-temperature superconducting wires, Adv. Mater. 20 (3) (2008) 391–407.
[10] B. Sahoo, K.L. Routray, B. Panda, D. Samal, D. Behera, Excess conductivity and magnetization of $CoFe_2O_4$ combined with $YBa_2Cu_3O_{7-\delta}$ as a superconductor, J. Phys. Chem. Solids 132 (2019) 187–196.
[11] J. Gutierrez, A. Llordes, J. Gazquez, M. Gibert, N. Roma, S. Ricart, , et al. X. Obradors, Strong isotropic flux pinning in solution-derived $YBa_2Cu_3O_{7-\delta}$ nanocomposite superconductor films, Nat. Mater. 6 (5) (2007) 367.
[12] R.A. Al-Mohsin, A.L. Al-Otaibi, M.A. Almessiere, H. Al-badairy, Y. Slimani, F. B. Azzouz, Comparison of the microstructure and flux pinning properties of polycrystalline $YBa_2Cu_3O_{7-d}$ containing $Zn_{0.95}Mn_{0.05}O$ or Al_2O_3 nanoparticles, J. Low Temp. Phys. (2018) 1–17.
[13] J. Jia, G. Zhao, L. Lei, Q. Huang, L. Liu, Fabrication of superconducting $YBa_2Cu_3O_{7-\delta}$ delay lines by a chemically modified sol-gel method, Ceram. Int. 41 (2) (2015) 2134–2139.
[14] S. Engel, T. Thersleff, R. Hühne, L. Schultz, B. Holzapfel, S. Engel, , et al.L. Schultz, Enhanced flux pinning in $YBa_2Cu_3O_7$layers by the formation of nanosized $BaHfO_3$ precipitates using the chemical deposition method, Appl. Phys. Lett. 90 (10) (2007) 102505.
[15] J. Gutierrez, A. Llordes, J. Gazquez, M. Gibert, N. Roma, S. Ricart, , et al. X. Obradors, Strong isotropic flux pinning in solution-derived $YBa_2Cu_3O_{7-\delta}$ nanocomposite superconductor films, Nat. Mater. 6 (5) (2007) 367.
[16] S.B. Guner, O. Gorur, S. Celik, M. Dogruer, G. Yildirim, A. Varilci, C. Terzioglu, Effect of zirconium diffusion on the microstructural and superconducting properties of $YBa_2Cu_3O_{7-\delta}$ superconductors, J. Alloy. Comp. 540 (2012) 260–266.
[17] S.X. Dou, W.K. Yeoh, J. Horvat, M. Ionescu, Effect of carbon nanotube doping on critical current density of MgB2 superconductor, Appl. Phys. Lett. 83 (2003) 4996.
[18] B. Sahoo, S.R. Mohapatra, A.K. Singh, D. Samal, D. Behera, Effects of CNTs blending on the superconducting parameters of YBCO superconductor, Ceram. Int. 45 (6) (2019) 7709–7716.
[19] N.A. Khalid, M.M.A. Kechik, N.A. Baharuddin, C.S. Kien, H. Baqiah, N.N.M. Yusuf, , et al.Z.A. Talib, Impact of carbon nanotubes addition on transport and superconducting properties of $YBa_2Cu_3O_{7-\delta}$ ceramics, Ceram. Int. 44 (8) (2018) 9568–9573.
[20] N.H. Mohammed, A.I. Abou-Aly, I.H. Ibrahim, R. Awad, M. Rekaby, Mechanical properties of $(Cu_{0.5}Tl_{0.5})$-1223 added by nano-SnO_2, J. Alloy. Comp. 486 (1–2) (2009) 733–737.
[21] N.H. Mohammed, A.I. Abou-Aly, I.H. Ibrahim, R. Awad, M. Rekaby, Effect of nano-oxides addition on the mechanical properties of $(Cu_{0.5}Tl_{0.5})$-1223 phase, J. Supercond. Nov. Magnetism 24 (5) (2011) 1463–1472.
[22] N.H. Mohammed, A.I. Abou-Aly, R. Awad, I.H. Ibrahim, M. Roumie, M. Rekaby, Mechanical and electrical properties of $(Cu_{0.5}Tl_{0.5})$-1223 phase added with nano-Fe_2O_3, J. Low Temp. Phys. 172 (3–4) (2013) 234–255.
[23] N.A. Hamid, M.Y.A. Rahman, N.F. Shamsudin, Mechanical and superconducting properties of nanosize MgO added dip-coated $Bi_2Sr_2CaCu_2O_8$ superconducting tape, Nat. Sci. 3 (6) (2011) 484–487.
[24] K. Konstantopoulou, Y.H. Shi, A.R. Dennis, J.H. Durrell, J.Y. Pastor, D.A. Cardwell, Mechanical characterization of GdBCO/Ag and YBCO single grains fabricated by top-seeded melt growth at 77 and 300 K, Supercond. Sci. Technol. 27 (11) (2014) 115011.
[25] N. Selvakumar, A. Biswas, S.B. Krupanidhi, H.C. Barshilia, Enhanced optical absorption of graphene-based heat mirror with tunable spectral selectivity", Sol. Energy Mater. Sol. Cells 186 (2018) 149–153.
[26] M. Vaqueiro-Contreras, C. Bartlam, R.S. Bonilla, V.P. Markevich, M.P. Halsall, A. Vijayaraghavan, A.R. Peaker, Graphene oxide films for field effect surface passivation of silicon for solar cells, Sol. Energy Mater. Sol. Cells 187 (2018) 189–193.
[27] S. Pei, H.M. Cheng, The reduction of graphene oxide, Carbon 50 (9) (2012) 3210–3228.

[28] K. Iida, N.H. Babu, E.S. Reddy, Y.-H. Shi, D.A. Cardwell, The effect of nano-size ZrO2 powder addition on the microstructure and superconducting properties of single-domain Y–Ba–Cu–O bulk superconductors, Supercond. Sci. Technol. 18 (3) (2005) 249.
[29] A. Jabbar, I. Qasim, K.M. Khan, Z. Ali, K. Nadeem, M. Mumtaz, Synthesis and superconducting properties of (Au) $_x$/CuTl-1223 composites, J. Alloy. Comp. 618 (2015) 110–114.
[30] C. Gómez-Navarro, R.T. Weitz, A.M. Bittner, M. Scolari, A. Mews, M. Burghard, K. Kern, Electronic transport properties of individual chemically reduced graphene oxide sheets, Nano Lett. 7 (11) (2007) 3499–3503.
[31] C. Gómez-Navarro, R.T. Weitz, A.M. Bittner, M. Scolari, A. Mews, M. Burghard, K. Kern, Electronic transport properties of individual chemically reduced graphene oxide sheets, Nano Lett. 9 (5) (2009), 2206-2206.
[32] Y. Bruynseraede, J. Vanacken, B. Wuyts, C. Van Haesendonck, J.P. Locquet, I. K. Schuller, Oxygen disorder effects in high Tc superconductors, Phys. Scr. 1989 (T29) (1989) 100.
[33] K.S.B. De Silva, S. Gambhir, X.L. Wang, X. Xu, W.X. Li, D.L. Officer, , et al.S.X. Dou, The effect of reduced graphene oxide addition on the superconductivity of MgB_2, J. Mater. Chem. 22 (28) (2012) 13941–13946.
[34] S. Dadras, S. Dehghani, M. Davoudiniya, S. Falahati, Improving superconducting properties of YBCO high temperature superconductor by Graphene Oxide doping, Mater. Chem. Phys. 193 (2017) 496–500.
[35] N.A. Khan, M. Mumtaz, Absence of a pair-breaking mechanism in $Cu_{0.5}Tl_{0.5}Ba_2Ca_3Cu_{4-y}Zn_yO_{12-\delta}$, Phys. Rev. B 77 (5) (2008), 054507.
[36] K. Nadeem, G. Hussain, M. Mumtaz, A. Haider, S. Ahmed, Role of magnetic NiFe2O4 nanoparticles in CuTl-1223 superconductor, Ceram. Int. 41 (10) (2015) 15041–15047.
[37] A. Mohanta, D. Behera, Fluctuation induced magneto-conductivity studies in $YBa_2Cu_3O_{7-\delta}$+ $xBaZrO_3$ composite high-Tc superconductors, Phys. C Supercond. 470 (4) (2010) 295–303.
[38] M. Sahoo, D. Behera, SCOPF analysis of $YBa_2Cu_3O_{7-\delta}$+ xCr_2O_3 superconductor composite, J. Phys. Chem. Solids 74 (7) (2013) 950–956.
[39] B. Sahoo, K.L. Routray, D. Samal, D. Behera, Effect of artificial pinning centers on YBCO high temperature superconductor through substitution of graphene nano-platelets, Mater. Chem. Phys. 223 (2019) 784–788.
[40] R. Awad, A.A. Aly, N.H. Mohammed, S. Isber, H.A. Motaweh, D.E.S. Bakeer, Investigation on superconducting properties of $GdBa_2Cu_3O_{7-\delta}$ added with nanosized $ZnFe_2O_4$, J. Alloy. Comp. 610 (2014) 614–622.
[41] H.A. Afifi, I.Z. Hager, N.S.A. Aal, A.M.A. El-Aziz, Study of the effect of Ni additive in $YBa_2Cu_3O_{7-\delta}$ superconducting composite employing ultrasonic measurement, Measurement 135 (2019) 928–934.
[42] I.Z. Hager, Effect of Er_2O_3 and ErF_3 on the structural and elastic properties of sodium oxyfluoroborate glasses, J. Alloy. Comp. 539 (2012) 256–263.
[43] Y. B. Saddeek, R. El-Mallawany, & H. Afifi, "Mechanical relaxation of some tellurovanadate glasses". J. Non-Cryst. Solids, 417, 28-33.
[44] M. Cankurtaran, G.A. Saunders, J.R. Willis, A. Al-Kheffaji, D.P. Almond, Bulk modulus and its pressure derivative of $YBa_2Cu_3O_{7-x}$, Phys. Rev. B 39 (4) (1989) 2872.
[45] M. Levy (Ed.), Ultrasonics of High-T [inferior C] and Other Unconventional Superconductors, Academic Press *Physical Acoustics*, 1992.
[46] Y. Horie, Y. Terashi, S. Mase, Ultrasonic studies and phonon modes of (RE) $Ba_2Cu_3O_7$, J. Phys. Soc. Jpn. 58 (1) (1989) 279–290.
[47] W. Malaeb, H. Basma, M.M. Barakat, R. Awad, Investigation of the mechanical properties of $GdBa_2Cu_3O_{7-\delta}$ added with nanosized ferrites ZnFe 2 O 4 and CoFe 2 O 4 using ultrasonic measurements, J. Supercond. Nov. Magnetism 30 (12) (2017) 3595–3602.
[48] S.P. Dodd, M. Cankurtaran, B. James, Ultrasonic determination of the elastic and nonlinear acoustic properties of transition-metal carbide ceramics: TiC and TaC, J. Mater. Sci. 38 (6) (2003) 1107–1115.
[49] M.B. Solunke, P.U. Sharma, M.P. Pandya, V.K. Lakhani, K.B. Modi, P.V. Reddy, S. S. Shah, Ultrasonic studies of aluminium-substituted Bi (Pb)-2223 superconductors, Pramana 65 (3) (2005) 481–490.
[50] R. Abd-Shukor, Acoustic Debye temperature and the role of phonons in cuprates and related superconductors, Supercond. Sci. Technol. 15 (3) (2002) 435.
[51] D.P. Almond, Q. Wang, J. Freestone, E.F. Lambson, B. Chapman, G.A. Saunders, An ultrasonic study of superconducting and non-superconducting $GdBa_2Cu_3O_{7-x}$, J. Phys. Condens. Matter 1 (38) (1989) 6853.